Bioorganic & Medicinal Chemistry Letters 19 (2009) 314–318

Contents lists available at ScienceDirect

Bioorganic & Medicinal Chemistry Letters

journal homepage: www.elsevier.com/locate/bmcl

CoMFA and CoMSIA 3D-QSAR studies on S^6-(4-nitrobenzyl)mercaptopurine riboside (NBMPR) analogs as inhibitors of human equilibrative nucleoside transporter 1 (hENT1)

Amol Gupte, John K. Buolamwini *

Department of Pharmaceutical Sciences, College of Pharmacy, University of Tennessee Health Sciences Center, 847 Monroe Avenue Suite 327, Memphis, TN 38163, USA

ARTICLE INFO

Article history:
Received 22 September 2008
Revised 20 November 2008
Accepted 24 November 2008
Available online 27 November 2008

Keywords:
Equilibrative nucleoside transporter
hENT1
Inhibitor
3D-QSAR
CoMFA
CoMSIA
Cross validation
NBMPR analogs

ABSTRACT

3D-QSAR (CoMFA and CoMSIA) studies were performed on human equlibrative nucleoside transporter (hENT1) inhibitors displaying K_i values ranging from 10,000 to 0.7 nM. Both CoMFA and CoMSIA analysis gave reliable models with q^2 values >0.50 and r^2 values >0.92. The models have been validated for their stability and robustness using group validation and bootstrapping techniques and for their predictive abilities using an external test set of nine compounds. The high predictive r^2 values of the test set (0.72 for CoMFA model and 0.74 for CoMSIA model) reveals that the models can prove to be a useful tool for activity prediction of newly designed nucleoside transporter inhibitors. The CoMFA and CoMSIA contour maps identify features important for exhibiting good binding affinities at the transporter, and can thus serve as a useful guide for the design of potential equilibrative nucleoside transporter inhibitors.

In humans, the cellular uptake and efflux of nucleosides is regulated by specialized transport proteins known as nucleoside transporters.[1] The potential of nucleoside transport inhibitors for therapeutic application in heart disease,[2] inflammatory disease,[3] viral infections,[4] and cancer chemotherapy[5,6] has been widely reported. Nucleoside transporters can be classified into two major classes, namely, the bidirectional sodium-independent equilibrative nucleoside transporters (ENTs)[7] and the unidirectional sodium dependent concentrative nucleoside transporters (CNTs).[8] In humans, four equilibrative nucleoside transporters[9–12] and six concentrative nucleoside transporters[13–16] have been identified. The ubiquitously distributed equlibrative nucleoside transporter hENT1, is the major nucleoside transporter in a number of mammalian tissues and appears to be the most relevant target for therapeutic exploitation. Although several chemical classes have been shown to inhibit the hENT1 protein none of them can be exploited for therapeutic application due to their poor pharmacological profiles with regard to toxicity, selectivity and poor in vivo efficacy.[16] Hence there is a pressing need for novel hENT1 inhibitors.

Amongst the known chemical classes of hENT1 inhibitors, S^6-(4-nitrobenzyl)mercaptopurine riboside (NBMPR, Fig. 1) and its congeners are the most potent and selective.[17] A recent publication

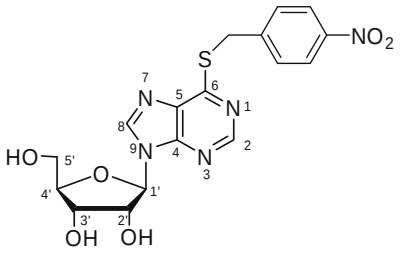

Figure 1. Structure of NBMPR.

from this laboratory reports a detailed study undertaken to derive a 3D pharmacophore model of the bioactive conformation of NBMPR at the hENT1 nucleoside transporter.[18] Earlier, in our attempts to develop novel nucleoside transport inhibitors based on the structure of NBMPR we had synthesized and evaluated a number of diverse S^6 position substituted[19,20] and C^2-purine substituted analogs[21] of NBMPR as hENT1 inhibitors. In this study, we have made use of the recently reported 3D pharmacophore derived bioactive conformation[18] to conduct 3D-QSAR studies involving CoMFA (comparative molecular field analysis) and CoMSIA (comparative molecular similarity indices analysis) using our previously reported S^6 substituted[19,20] and C^2-purine substituted NBMPR analogs[21] enlisted in Table 1. In addition to revalidating

* Corresponding author. Tel.: +1 901 448 7533; fax: +901 448 6828.
E-mail address: jbuolamwini@utmem.edu (J.K. Buolamwini).

0960-894X/$ - see front matter © 2008 Elsevier Ltd. All rights reserved.
doi:10.1016/j.bmcl.2008.11.092

Table 1
Structures and inhibitory activities of compounds used for 3D-QSAR studies

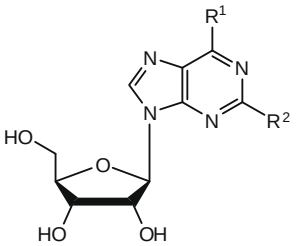

Compound	R^1	R^2	pK_i[a]	Compound	R^1	R^2	pK_i[a]
1	–*S*-(4-Nitrobenzyl)	–H	9.15[b]	**27**	–*S*-(4-*tert*-butylbenzyl)	–H	5.00[d]
2	–*S*-(4-Nitrobenzyl)	$-NH_2$	8.96[c]	**28**	–*S*-(4-Methoxycarbonylbenzyl)	–H	7.33[d]
3	–*S*-(2-Fluorobenzyl)	–H	7.62[b]	**29**	–*S*-(2,4-Dichlorobenzyl)	–H	8.36[d]
4	–*S*-(3-Fluorobenzyl)	–H	7.89[b]	**30**	–*S*-(3,4-Dichlorobenzyl)	–H	7.90[d]
5	–*S*-(4-Fluorobenzyl)	–H	8.04[b]	**31**	–*S*-(2-Chloro-6-Fluorobenzyl)	–H	7.06[d]
6	–*S*-(2-Chlorobenzyl)	–H	6.93[b]	**32**	–*S*-(2,4,6-Trimethylbenzyl)	–H	5.72[d]
7	–*S*-(3-Chlorobenzyl)	–H	7.74[b]	**33**	–*S*-(4-Nitrobenzyl)	–F	8.67[c]
8	–*S*-(4-Chlorobenzyl)	–H	7.83[b]	**34**	–*S*-(4-Nitrobenzyl)	–Cl	7.96[c]
9	–*S*-(2-Bromobenzyl)	–H	6.82[b]	**35**	–*S*-(4-Nitrobenzyl)	–Br	7.94[c]
10	–*S*-(3-Bromobenzyl)	–H	7.68[b]	**36**	–*S*-(4-Nitrobenzyl)	–I	7.92[c]
11	–*S*-(4-Bromobenzyl)	–H	7.94[b]	**37**	–*S*-(4-Nitrobenzyl)	$-NHCH_3$	7.62[c]
12	–*S*-(2-Iodobenzyl)	–H	7.71[b]	**38**	–*S*-(4-Nitrobenzyl)	$-N(CH_3)_2$	6.37[c]
13	–*S*-(3-Iodobenzyl)	–H	7.86[b]	**39**	–*S*-(4-Nitrobenzyl)	$-NHCH_2CH_3$	7.60[c]
14	–*S*-(4-Iodobenzyl)	–H	8.42[b]	**40**	–*S*-(4-Nitrobenzyl)	$-NHCH_2CH_2CH_3$	6.71[c]
15	–*S*-(2-Cyanobenzyl)	–H	7.41[e]	**41**	–*S*-(4-Nitrobenzyl)	–NH-cyclopropyl	7.60[c]
16	–*S*-(3-Cyanobenzyl)	–H	7.44[e]	**42**	–*S*-(4-Nitrobenzyl)	$-NHCH_2CH_2CH_2CH_3$	6.49[c]
17	–*S*-(4-Cyanobenzyl)	–H	8.34[d]	**43**	–*S*-(4-Nitrobenzyl)	–NH-cyclobutyl	7.48[c]
18	–*S*-(2-Nitrobenzyl)	–H	6.94[e]	**44**	–*S*-(4-Nitrobenzyl)	$-NHCH_2CH_2CH_2CH_2CH_3$	6.45[c]
19	–*S*-Benzyl	–H	7.70[d]	**45**	–*S*-(4-Nitrobenzyl)	–NH-cyclopentyl	6.90[c]
20	–*S*-(3-Nitrobenzyl)	–H	8.75[d]	**46**	–*S*-(4-Nitrobenzyl)	–NH-cyclohexyl	6.40[c]
21	–*S*-(2-Methylbenzyl)	–H	7.17[d]	**47**	–*S*-(4-Nitrobenzyl)	$-NHCH_2C_6H_5$	6.61[c]
22	–*S*-(3-Methylbenzyl)	–H	7.79[d]	**48**	–*S*-(4-Nitrobenzyl)	$-NHCH_2CH_2C_6H_5$	6.40[c]
23	–*S*-(4-Methylbenzyl)	–H	7.82[d]	**49**	–*S*-(4-Nitrobenzyl)	$-NHCH_2CH_2OH$	7.06[c]
24	–*S*-(3-Trifluoromethylbenzyl)	–H	7.72[d]	**50**	–*S*-(4-Nitrobenzyl)	$-N(CH_2CH_2OH)$	6.61[c]
25	–*S*-(4-Methoxybenzyl)	–H	7.46[d]	**51**	–*S*-(4-Nitrobenzyl)	$-NHC(O)CH_3$	7.47[c]
26	–*S*-(4-Trifluoromethoxybenzyl)	–H	8.15[d]	**52**	–*S*-(4-Nitrobenzyl)	$-NHC(O)C_6H_5$	6.50[c]

[a] $pK_i = -\log_{10}K_i$.
[b] Results taken from literature.[19]
[c] Results taken from literature.[21]
[d] Results taken from literature.[20]

the 3D pharmacophore derived bioactive conformation published earlier, the 3D-QSAR efforts would also decide the substituent properties of these compounds and provide a rationale for the design of novel inhibitors that can have therapeutic application.

All ligand structures were built using the previously published 3D pharmacophore model[18] of the bioactive conformation of NBMPR at the hENT1 nucleoside transporter. The pharmacophore model consists of six features—three hydrogen bond acceptors, one hydrophobic group, and two aromatic rings. In NBMPR the three hydrogen bond acceptor functions are mapped onto the 3′-OH, the ribose ring oxygen, and the nitro group, the hydrophobic function is mapped onto the S^6-benzyl ring, and the two aromatic groups are mapped onto the purine system. According to the studies conducted for pharmacophore development NBMPR adopts an *anti* conformation, suggesting the anti-conformation to be the bioactive conformation of NBMPR and its analogs for binding to the hENT1 nucleoside transporter.[18]

A total of fifty-two compounds exhibiting nucleoside transporter inhibitory activities with K_i values in the range of 0.7–10,000 nM were used to carry out the 3D-QSAR analysis (Table 1). Three-dimensional structure building and all modeling operations were performed using SYBYL 7.2 (Tripos Associates Inc.) on a Silicon Graphics Octane workstation. Partial atomic charges were calculated using the MOPAC-PM3 algorithm. Energy minimization was performed using Tripos force field with a distance-dependent dielectric and the BFGS algorithm, with a convergence criterion of 0.01 kcal/(mol Å). The compounds in training set were aligned using MATCH module in SYBYL. The reference atoms selected for alignment and the alignment of all molecules is shown in Figure 2.

The fifty-two compounds were divided into a training set comprising 43 compounds and an external test set comprising nine compounds. The test set consists of compounds **9, 17, 18, 22, 33, 34, 41, 44**, and **46**. The test set was chosen such that it represents the structural diversity and wide range of activity present in the entire data set. The K_i values were transformed into pK_i ($-\log K_i$) values and used as the dependent variable in CoMFA and CoMSIA analysis.

For deriving the CoMFA and CoMSIA descriptor fields, the molecules from the training set were placed in a three dimensional cubic lattice with a spacing of 2 Å and extending 4 Å units beyond the aligned molecules in all directions. CoMFA descriptors were calculated using an sp^3 carbon probe atom with a van der Waals radius of 1.52 Å and a charge of +1.0 with a distance-dependent dielectric to generate steric (Lennard-Jones 6–12 potential) field energies and electrostatic (Coulombic potential) fields with a distance-dependent dielectric at each lattice point. An energy cutoff of 30 kcal/mol was applied. The CoMFA steric and electrostatic fields were scaled by the CoMFA-STD method in SYBYL.

CoMSIA similarity index descriptors were calculated using a similar lattice box as in CoMFA. CoMSIA similarity indices descriptors were derived according to Klebe et. al. The CoMSIA descriptors, namely, steric, electrostatic, hydrophobic, hydrogen bond donor,

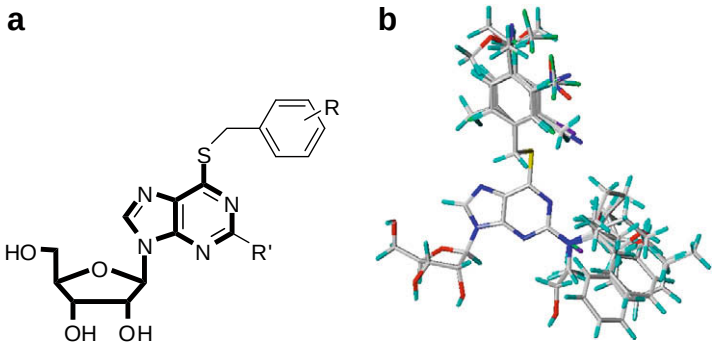

Figure 2. (a) Atoms used in MATCH alignments shown in bold face on a general structure. (b) Alignment of all molecules: Blue indicates nitrogen, red indicates oxygen, yellow refers to sulfur, gray indicates carbon, and cyan indicates hydrogen.

and hydrogen bond acceptor, were generated using a sp^3 carbon probe atom with +1.0 charge and a van der Waals radius of 1.4 Å. CoMSIA similarity indices ($A_{F,k}$) between a molecule j and atoms i at a grid point were calculated by using Eq. 1 as follows:

$$A^q_{F,k}(j) = -\sum \omega_{\text{probe},k}\omega_{ik}e^{-ar}iq^2 \quad (1)$$

Five physicochemical properties or descriptors (k), steric, electrostatic, hydrophobic, hydrogen bond donor and hydrogen bond acceptor were evaluated. The descriptor k of atom i is ω_{ik}, while the descriptor of the probe atom is ω_{probe}. A Gaussian-type distance dependence was used between the grid point q and each atom i in the molecule. The value of the attenuation factor (α) was set to 0.3. The CoMSIA steric indices are related to the third power of the atomic radii, the electrostatic descriptors are derived from atomic partial charges, the hydrophobic fields are derived from atom-based parameters developed by Viswanadhan et. al.,[22] and hydrogen bond donor and acceptor indices are obtained from a rule based method derived from experimental data.[23]

Using CoMFA and CoMSIA descriptors as independent variables and pK_i values as dependent variables, partial least squares (PLS) regression analyses were carried out, using QSAR module of the SYBYL package with default parameters. Leave-one-out (LOO) cross-validation was used to evaluate the predictive ability of the models. The cross-validated coefficient, q^2, was calculated using Eq. 2 as follows:

$$q^2 = 1 - \frac{\sum(Y_{\text{predicted}} - Y_{\text{actual}})^2}{\sum(Y_{\text{observed}} - Y_{\text{mean}})^2} \quad (2)$$

where $Y_{\text{predicted}}$, Y_{actual}, and Y_{mean} are predicted, actual and mean values of the target property (pK_i), respectively. $\Sigma(Y_{\text{predicted}} - Y_{\text{actual}})^2$ is the predictive sum of squares (PRESS). The optimum number of components used to derive the final regression models was the one that corresponds to the lowest PRESS value.[24] In addition to the q^2, the corresponding PRESS, the conventional correlation coefficient (r^2) and its standard error (s) were also computed. To test the stability and robustness of the models, more rigorous statistical testing was performed by group cross-validation (10 groups, 30 runs) and bootstrapping (30 runs). To eliminate the possibility of chance correlation, PLS analysis was carried out using scrambled activity data (20 runs). CoMFA and CoMSIA coefficient maps were generated by interpolation of the pairwise products between the PLS coefficients and the standard deviations of the corresponding CoMFA and CoMSIA descriptor values.

In this study, CoMFA and CoMSIA 3D-QSAR analysis were undertaken to determine the effects of steric, electrostatic, hydrophobic, and hydrogen bonding properties of the compounds on hENT1 nucleoside transporter inhibitory activity, and to obtain reliable models for predicting the activity of compounds belonging to a similar structural class. The results obtained from PLS regression analysis, using the CoMFA and CoMSIA descriptors as independent variables are shown in Table 2. Initial CoMFA and CoMSIA PLS analyses with all 43 compounds in the training set afforded models with very low q^2 values. A CoMFA model with a q^2 value of 0.643 and a CoMSIA model with a q^2 value of 0.513 were obtained after removing three possible outliers for the CoMFA model and four for the CoMSIA model. Three of these outliers, compound 27, compound 28, and compound 32 were common to both the CoMFA and CoMSIA models. Compound 27, with a *para-tert*-butyl substituent, has a reported K_i value of >10,000 nM. It does not have an accurate K_i value and Compound 32 is unique to the set considering that it is the only compound with a tri-substituted S^6-benzyl group. Compound 38 was an additional outlier removed to obtain a reasonable CoMSIA model. Compound 38, the dimethyl substituted C^2-position analog, is the only dialkyl substituted compound in the series and this might explain its outlier status.

The stability of the CoMFA and CoMSIA models was evaluated by performing group cross-validation (30 runs) and bootstrapping (30 runs). The results of these validations are shown in Table 3. The robustness of these models was demonstrated by q^2 and r^2 values, respectively, obtained from group cross-validation and bootstrapping which are not very distinct from the original values. The possibility of a chance correlation between the CoMFA and CoMSIA descriptors, and biological activity was also eliminated after performing PLS analysis using randomizations (20 runs).

Activity (pK_i) values for the compounds in the training set were predicted using the final CoMFA and CoMSIA models. The predictive abilities of the models were evaluated against an external test set (9 compounds). Both the CoMFA and CoMSIA models predicted pK_i values of the test set lie within a one log unit limit (Fig. 3 and Table 4).

Table 2
PLS statistics of CoMFA and CoMSIA 3D-QSAR models

PLS statistics[a]	CoMFA model	CoMSIA model
q^2	0.643	0.513
PRESS	0.434	0.486
r^2	0.943	0.929
s	0.177	0.191
F	90.171	69.818
PLS components	5	4
Field contribution		
Steric	0.635	0.125
Electrostatic	0.365	0.210
Hydrophobic		0.381
Donor		0.126
Acceptor		0.163

[a] q^2, cross-validated correlation coefficient; PRESS, predictive sum of squares; s, standard error; r^2, correlation coefficient; F, F-test value.

Table 3
Results of group cross-validation, randomizations and bootstrapping

Exercise	PLS statistics	CoMFA[a]	CoMSIA[a]
Group validation[b]	q^2	0.631 (0.030)	0.506 (0.040)
Randomization[c]	q^2	−0.155	−0.101
Bootstrapping[b]	r^2	0.962 (0.007)	0.938 (0.008)
	s	0.170 (0.0134)	0.026 (0.006)

[a] Values in parentheses are standard deviations.
[b] Average of 30 runs.
[c] Average of 20 runs.

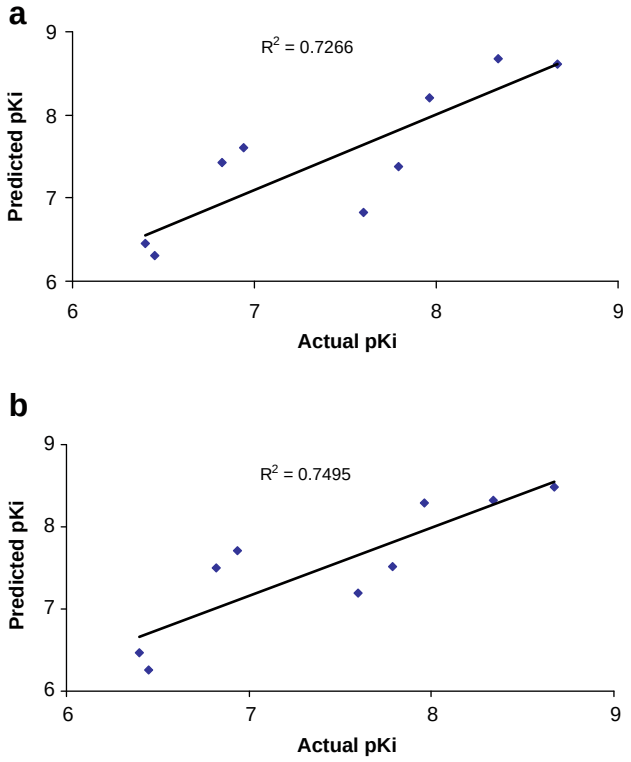

Figure 3. Prediction curves for CoMFA (a) or CoMSIA (b) model-predicted pK_i values for the test set of ENT1 inhibitors.

Contour maps were generated by plotting the coefficients from CoMFA and CoMSIA QSAR models, which indicate regions in 3D space around the molecules where changes in the particular physicochemical properties are predicted to increase or decrease potency. The steric and electrostatic contours for CoMFA and CoMSIA models projected unto NBMPR are shown in Figure 4, and hydrophobic and hydrogen bond contours for the CoMSIA model for ENT1 transporter inhibition, also projected unto NBMPR are shown in Figure 5.

A yellow contour near the C^2-purine position indicates that a bulky substituent at this site decreases binding affinity at the hENT1 transporter (Fig. 4a). This is consistent with the fact that within the straight chain alkylamine substituents we observe an increase in the K_i values as the carbon chain length increases. A smaller green contour near the *para*- position of the S^6-benzyl substituent indicates that steric bulk is favored at this site. The presence of a red contour near the *para -position* of the S^6-benzyl substituent indicates that negative electrostatic potential around this region increases the binding affinity. The presence of a blue contour near the C^2-purine position yellow contour indicates that smaller electron deficient groups at this site might enhance the binding affinity at the hENT1 transporter.

In general, the CoMSIA steric and electrostatic plots agree well with the CoMFA plots (Fig. 4b). The orange contour in the CoMSIA hydrophobic plot indicates that hydrophobic groups at the C^2-position and around the S^6-benzyl group are disfavored (Fig. 5a). A green contour around the *para*-position of the S^6-benzyl substituent indicates that hydrophobic groups are tolerated at this position. The presence of both the hydrophobic favored and disfavored contours around the same region indicates that a balance of these properties among the groups present at this region is required for optimum binding at the hENT1 transporter. The cyan contour near the C^2-purine position shows that a hydrogen bond donor is favored at this location (Fig. 5b). The NH on the C^2-alkylamine substituents might be involved in hydrogen bonding at the binding site. On the other hand, a prominent magenta colored contour near the para-position of the S^6-benzyl substituent indicates that a hydrogen bond acceptor is favored at this position (Fig. 5b). The purple and red contours indicate the presence of a hydrogen bond donor and acceptor disfavored regions, respectively. However, these groups do not appear to have a major influence in the binding of these molecules to the hENT1 transporter.

In this study, a pharmacophore hypothesis published earlier[18] has been used to develop 3D-QSAR CoMFA and CoMSIA models. The models developed have been validated for their stability and robustness using group validation and bootstrapping techniques and for their predictive abilities using an external test set. The models rationalize the binding data at the hENT1 nucleoside transporter and help understand the features important for exhibiting good binding affinities at the transporter.

The PLS coefficient contour maps have highlighted the importance of a hydrogen bond donor and the presence of steric and hydrophobic restrictions at the C^2-purine position. The presence of a hydrogen bond acceptor around the *para*-position of S^6-benzyl substituent has been demonstrated to be important for good binding at the hENT1 transporter. A balance between the hydrophobic favored and disfavored properties at this region is necessary for displaying good binding affinities at the transporter. A negative electrostatic potential in the same region also improves the binding affinities of compounds at the transporter. The mapping of these

Table 4
Residuals of predictions of the test set by the CoMFA and CoMSIA models

Compound	Actual pK_i[a]	Predicted CoMFA pK_i[a]	CoMFA residuals	Predicted CoMSIA pK_i[a]	CoMSIA residuals
9	6.82	7.41	−0.59	7.49	−0.67
17	8.34	8.67	−0.33	8.31	0.03
18	6.94	7.60	−0.66	7.71	−0.77
22	7.79	7.37	0.42	7.52	0.27
33	8.67	8.61	0.06	8.48	0.19
34	7.96	8.19	−0.23	8.29	−0.33
41	7.60	6.83	0.77	7.18	0.42
44	6.45	6.30	0.15	6.25	0.20
46	6.40	6.45	−0.05	6.46	0.06

[a] pK_i = $-\log_{10}K_i$.

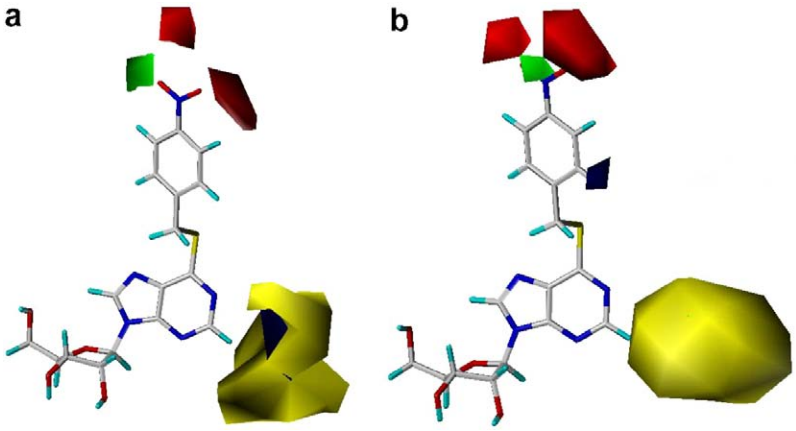

Figure 4. PLS contours from 3D-QSAR models for ENT1 transporter inhibitors. (a) Steric and electrostatic CoMFA contours; (b) Steric and electrostatic CoMSIA contours. The green contours indicate sterically favored regions whereas the yellow contours denote sterically unfavorable regions. The blue contours identify regions that favor electropositive substituents and the red regions favor electronegative substituents.

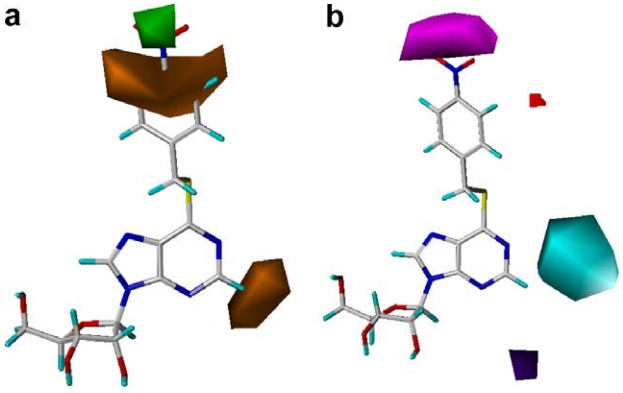

Figure 5. PLS contours from 3D-QSAR models for ENT1 transporter inhibitors. (a) Hydrophobic CoMSIA contours; (b) Hydrogen bond donor/acceptor CoMSIA contours. The green contours indicate regions where hydrophobic groups are favored whereas the orange contours denote regions that disfavor hydrophobic groups. The cyan and purple contours indicate favorable and unfavorable regions for hydrogen bond donors, respectively. The magenta and red contours identify favorable and unfavorable positions for hydrogen bond acceptors, respectively.

properties would prove useful in better inhibitor design. The obtained models can be used to predict the activity of newer analogs.

References and notes

1. Jacquez, J. A. *Biochim. Biophys. Acta* **1962**, *61*, 265.
2. Van Belle, H. *Cardiovasc. Res.* **1993**, *27*, 68.
3. Le Vraux, V.; Chen, Y. L.; Masson, I.; De Sousa, M.; Giroud, J. P.; Florentin, I.; Chauvelot-Moachon, L. *Life Sci.* **1993**, *52*, 1917.
4. Hendrix, C. W.; Flexner, C.; Szebeni, J.; Kuwahara, S.; Pennypacker, S.; Weinstein, J. N.; Lietman, P. S. *Antimicrob. Agents Chemother.* **1994**, *38*, 1036.
5. Weber, G.; Lui, M. S.; Natsumeda, Y.; Faderan, M. A. *Adv. Enzyme Regul.* **1983**, *21*, 53.
6. Weber, G.; Jayaram, H. N.; Pillwein, K.; Natsumeda, Y.; Reardon, M. A.; Zhen, Y. S. *Adv. Enzyme Regul.* **1987**, *26*, 335.
7. Baldwin, S. A.; Beal, P. R.; Yao, S. Y.; King, A. E.; Cass, C. E.; Young, J. D. *Pflugers Arch.* **2004**, *447*, 735.
8. Gray, J. H.; Owen, R. P.; Giacomini, K. M. *Pflugers Arch.* **2004**, *447*, 728.
9. Griffiths, M.; Beaumont, N.; Yao, S. Y.; Sundaram, M.; Boumah, C. E.; Davies, A.; Kwong, F. Y.; Coe, I.; Cass, C. E.; Young, J. D.; Baldwin, S. A. *Nat. Med.* **1997**, *3*, 89.
10. Griffiths, M.; Yao, S. Y.; Abidi, F.; Phillips, S. E.; Cass, C. E.; Young, J. D.; Baldwin, S. A. *Biochem. J.* **1997**, *328*, 739.
11. Baldwin, S. A.; Yao, S. Y.; Hyde, R. J.; Ng, A. M.; Foppolo, S.; Barnes, K.; Ritzel, M. W.; Cass, C. E.; Young, J. D. *J. Biol. Chem.* **2005**, *280*, 15880.
12. Barnes, K.; Dobrzynski, H.; Foppolo, S.; Beal, P. R.; Ismat, F.; Scullion, E. R.; Sun, L.; Tellez, J.; Ritzel, M. W.; Claycomb, W. C.; Cass, C. E.; Young, J. D.; Billeter-Clark, R.; Boyett, M. R.; Baldwin, S. A. *Circ. Res.* **2006**, *99*, 510.
13. Huang, Q. Q.; Yao, S. Y.; Ritzel, M. W.; Paterson, A. R.; Cass, C. E.; Young, J. D. *J. Biol. Chem.* **1994**, *269*, 17757.
14. Wang, J.; Su, S. F.; Dresser, M. J.; Schaner, M. E.; Washington, C. B.; Giacomini, K. M. *Am. J. Physiol.* **1997**, *273*, F1058.
15. Ritzel, M. W.; Ng, A. M.; Yao, S. Y.; Graham, K.; Loewen, S. K.; Smith, K. M.; Ritzel, R. G.; Mowles, D. A.; Carpenter, P.; Chen, X. Z.; Karpinski, E.; Hyde, R. J.; Baldwin, S. A.; Cass, C. E.; Young, J. D. *J. Biol. Chem.* **2001**, *276*, 2914.
16. Buolamwini, J. K. *Curr. Med. Chem.* **1997**, *4*, 35.
17. Cass, C. E. Drug Transport in Antimicrobial and Anticancer Chemotherapy;. In Georgopapadakou, N. H., Ed.; Marcel Dekker: New York, 1995; pp 403–451.
18. Zhu, Z.; Buolamwini, J. K. *Bioorg. Med. Chem.* **2008**, *16*, 3848.
19. Gupte, A.; Buolamwini, J. K. *Bioorg. Med. Chem. Lett.* **2004**, *14*, 2257.
20. Gupte, A.; Buolamwini, J. K.; Yadav, V.; Chu, C. K.; Naguib, F. N.; el Kouni, M. H. *Biochem. Pharmacol.* **2005**, *71*, 69.
21. Gupte, A.; Buolamwini, J. K. *Bioorg. Med. Chem.* **2007**, *15*, 7726.
22. Viswanadhan, V. N.; Ghose, A. K.; Revenkar, G. R.; Robins, R. K. *J. Chem. Inf. Comput. Sci.* **1989**, *29*, 163.
23. Klebe, G. *J. Mol. Biol.* **1994**, *237*, 212.
24. Buolamwini, J. K.; Raghavan, K.; Fesen, M. R.; Pommier, Y.; Kohn, K. W.; Weinstein, J. N. *Pharm. Res.* **1996**, *13*, 1891.